Mn-doped monolayer MoS_2: An atomically thin dilute magnetic semiconductor

Ashwin Ramasubramaniam*
Department of Mechanical and Industrial Engineering, University of Massachusetts Amherst, Amherst, Massachusetts 01003, USA

Doron Naveh†
Faculty of Engineering, Bar-Ilan University, Ramat-Gan 52900, Israel

(Received 21 March 2013; revised manuscript received 30 April 2013; published 13 May 2013)

We investigate the electronic and magnetic properties of Mn-doped monolayer MoS_2 using a combination of first-principles density functional theory (DFT) calculations and Monte Carlo simulations. Mn dopants that are substitutionally inserted at Mo sites are shown to couple ferromagnetically via a double-exchange mechanism. This interaction is relatively short ranged, making percolation a key factor in controlling long-range magnetic order. The DFT results are parameterized using an empirical model to facilitate Monte Carlo studies of concentration- and temperature-dependent ordering in these systems, through which we obtain Curie temperatures in excess of room temperature for Mn doping in the range of 10–15%. Our studies demonstrate the potential for engineering a new class of atomically thin dilute magnetic semiconductors based on Mn-doped MoS_2 monolayers.

DOI: 10.1103/PhysRevB.87.195201 PACS number(s): 73.22.−f, 75.50.Pp

I. INTRODUCTION

Dilute magnetic semiconductors (DMSs) have been the focus of extensive research over the last decade, driven by the prospect of realizing a new generation of electronic devices—so-called spintronic devices—that can exploit both the charge and spin of carriers.[1–4] To this end, a significant amount of theoretical and experimental effort has been devoted to understanding the role of magnetic impurities such as Mn and Co in technologically important III-V and II-VI semiconductors, as discussed in several reviews.[1–5] Among several challenges that persist in the development of spintronic devices, perhaps the most significant hurdle remains the control of the ordering temperature, which should ideally be well above room temperature to enable practical applications. The search for such room-temperature DMSs remains an active quest spanning a wide class of materials (e.g., III-Vs, II-VIs, oxides, half-Heusler alloys).[4]

The purpose of this paper is to extend the search for room-temperature DMSs to a relatively unexplored class of materials, the layered transition-metal dichalcogenides (TMDs). These materials have been the focus of much recent attention as they can be readily exfoliated to yield atomically thin layers for nanoelectronics, much like graphene. Notably, unlike graphene, several of these layered TMDs are semiconducting,[6–8] which makes them serious candidates for digital electronics. Recent demonstrations of MoS_2 devices such as field-effect transistors,[9,10] logic circuits,[11] and phototransistors[12] are already promising. With respect to magnetic properties, there have been recent experimental reports of magnetism in MoS_2 nanosheets, attributed to the presence of magnetic edge states;[13] irradiated MoS_2, attributed to a combination of point defects and edge states;[14] and in MoS_2 single crystals, attributed to zigzag edges at grain boundaries.[15] Theoretical calculations also provide evidence for magnetic ordering at edges of nanoribbons[16,17] and nanoflakes,[18] as well as defect and dopant-induced magnetism.[19] We are unaware of any systematic studies of magnetism in layered TMDs via substitutional doping of magnetic transition-metal atoms, which is the focus of this work.

In the following, we explore the effect of substitutional Mn doping in MoS_2 monolayers—in analogy with the commonly-used strategy in III-V and II-VI DMSs—and examine the potential for development of MoS_2-based DMSs. To this end, we employ first-principles density functional theory (DFT) calculations to first understand the electronic origins of ferromagnetic interactions between substitutional Mn dopant atoms and, thereafter, to parametrize a Monte Carlo (MC) model, which we employ for temperature-dependent studies of magnetic ordering in Mn-doped MoS_2 monolayers. We demonstrate that exchange interactions in Mn/MoS_2 DMSs are primarily governed by the double-exchange mechanism and are relatively short ranged, making percolation a key factor in magnetic ordering. Based on our DFT-parameterized MC simulations, we suggest that dopant concentrations in the range of 10–15% might be sufficient to provide room-temperature ferromagnetism in Mn/MoS_2 DMSs, paving the way for experimental verification and application in spintronic devices.

II. RESULTS AND DISCUSSION

A. Electronic structure calculations

First-principles calculations were performed using the Vienna *ab initio* package (VASP)[20] at two different levels of theory: standard Kohn-Sham DFT with the Perdew-Burke-Ernzerhof (PBE) exchange-correlation (XC) functional[21] and hybrid DFT using the Heyd-Scuseria-Ernzerhof (HSE) exchange correlation functional.[22] A detailed description of the DFT calculations is provided in the Appendix. Semilocal XC functionals, such as PBE, are known to suffer from self-interaction errors, which lead to excessive delocalization of the electronic wave functions. Such artifacts become particularly apparent when treating the *d* electrons of Mn and Mo as the occupied *d* states appear at excessively high energies, altering both the precise mechanism as well as the range of exchange interactions. Various strategies have been adopted in the literature to mitigate these self-interaction errors in DMSs; we refer the reader to the review in Ref. 4 and the references

therein. Here, we have chosen to employ the HSE functional, which reduces the self-interaction error by incorporating a fraction of exact exchange, leading to a better description of the electronic wave functions.[23] For monolayer MoS_2, in particular, the fundamental gap from HSE calculations appears to approximate the optical gap of the material.[7,24] In the following, we will compare and contrast the electronic structure of Mn dopants in monolayer MoS_2 using both the PBE and HSE functionals, and, furthermore, examine the influence of the electronic structure on the exchange coupling and Curie temperature of the resulting DMSs.

Before examining interactions between multiple Mn dopant atoms, we consider first the electronic structure of a single substitutional Mn atom in monolayer MoS_2. Figures 1(a) and 1(b) display the spin density ($\rho^{\uparrow} - \rho^{\downarrow}$) for a single substitutional Mn atom in a 4×4 supercell of monolayer MoS_2. The overall magnetic moment of the supercell is 1 μ_B corresponding to the single excess d electron provided by the Mn atom. From the bond lengths listed in Fig. 1(b), it is clear that there is a loss of D_{3h} (trigonal prism) symmetry at the Mn dopant site.[25] A significant portion of the spin density is localized on the Mn atom. The neighboring S atoms (labeled S_1 and S_2) are antiferromagnetically coupled to the Mn dopant; the p character of the spin-polarized orbitals of the S atoms is clearly visible. Out of the six Mo atoms that were originally the nearest neighbors of the dopant site, only the four closest Mo atoms (labeled Mo_2 and Mo_3) couple antiferromagnetically to the Mn atom while the two most distant ones (labeled Mo_1) couple ferromagnetically to the Mn atom. We attribute this difference in magnetic coupling to the loss of trigonal symmetry at the Mn dopant site upon atomic relaxation. While the general features noted thus far are similar in both the PBE and HSE cases, there are distinct differences, the most obvious being the extent of spin polarization in the vicinity of the Mn dopant. Specifically, by projecting the spin density onto atomic orbitals and integrating over the PAW sphere, we obtain a local magnetic moment of 1.04 μ_B and 2.77 μ_B on the Mn atom at the PBE and HSE levels, respectively. This suggests that the Mn(IV) atom adopts a low-spin d^3 configuration at the PBE level, while the HSE functional prefers a high-spin d^3 configuration, which explains the greater extent of spin polarization in the immediate vicinity of the Mn atom in the latter case.

Additional insight into the electronic structure of the Mn-doped MoS_2 monolayer can be obtained from the electronic density of states (DOS) displayed in Figs. 2(a) and 2(b). Within ligand-field theory, the trigonal prismatic coordination of the Mo atom lifts the degeneracy of the Mo 4d levels. The lowest-energy band is of Mo $4d_{z^2}$ character and is fully occupied; next in energy are degenerate, unoccupied Mo $4d_{xy}$ and Mo $4d_{x^2-y^2}$ bands, followed by the degenerate Mo $4d_{zx}$ and Mo $4d_{yz}$ bands of highest energy.[6,26] Experiments and first-principles calculations, suggest a more nuanced picture wherein hybridization occurs between the Mo $4d_{z^2}$, d_{xy}, $d_{x^2-y^2}$, and S $3p$ orbitals; these hybridized states dominate the conduction and valence band edges of MoS_2.[6,27–32] The

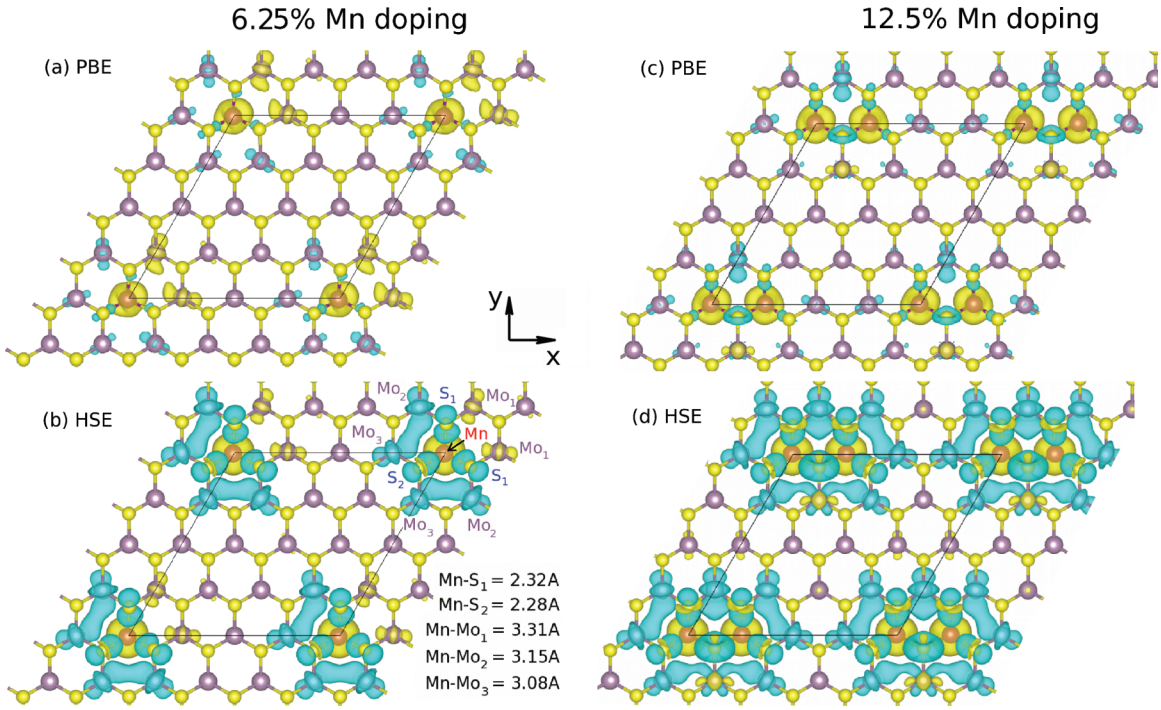

FIG. 1. (Color online) (a), (b) Spin density ($\rho^{\uparrow} - \rho^{\downarrow}$) for a single Mn dopant atom in a 4×4 monolayer MoS_2 supercell (6.25% Mn doping) and (c), (d) for two first-nearest-neighbor Mn dopants in the same supercell (12.5% Mn doping; ferromagnetic ground state). Yellow and cyan isosurfaces represent positive and negative spin densities (± 0.054 e/Å^3), respectively. At 6.25% doping, the dopant Mn atom has a local magnetic moment of 1.04 μ_B and 2.77 μ_B at the PBE and HSE levels, respectively. At 12.5% doping, the average local moments of the Mn atoms are 1.32 μ_B and 2.86 μ_B at the PBE and HSE levels, respectively. The S atoms that are bonded to the Mn atom, as well as several of the Mo atoms in the immediate vicinity of the Mn atom, display antiferromagnetic coupling to the dopant.

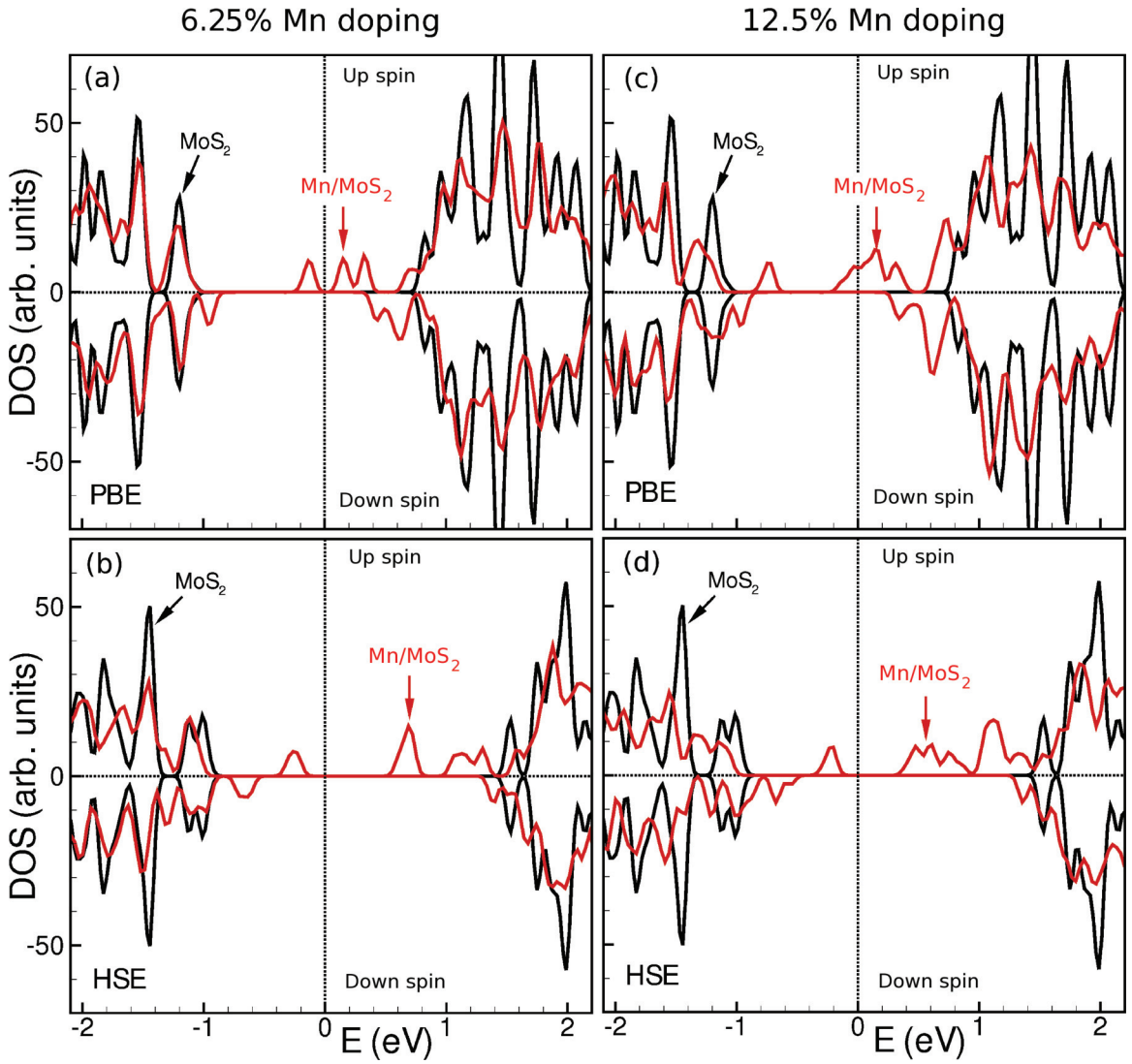

FIG. 2. (Color online) Density of states (DOS) for (a), (b) 6.25% Mn-doped and (c), (d) 12.5% Mn-doped monolayer MoS_2 calculated using PBE and HSE functionals. The Fermi level of the doped monolayer is set as the zero of the energy scale. The semicore $4p$ states of the undoped and doped monolayers (∼35 eV below the Fermi level) are aligned to clearly show the emergence of gap states in the doped monolayer. At the HSE level the monolayer remains semiconducting in both spin channels for both dopant concentrations. At the PBE level, the monolayer becomes half-metallic at 12.5% Mn doping.

fundamental band gap of the monolayer is 1.6 eV with the PBE and 2.05 eV with the HSE functional.[7] Upon substituting an Mo(IV) d^2 atom by an Mn(IV) d^3 atom, the degeneracy of the spin channels is broken and defect levels are formed within the MoS_2 band gap (Fig. 2). An analysis of the atom-projected DOS, displayed in the Supplementary Material,[33] reveals that the primary contributions to these gap states arise from the $4d_{z^2}$, $4d_{xy}$, and $4d_{x^2-y^2}$ states of the Mn atom and its neighboring spin-polarized Mo atoms, as well as the $3p$ states of the spin-polarized S atoms. The PBE DOS shows a negligible gap in the majority spin channel while the minority spin channel continues to display an appreciable gap, indicating that the doped monolayer is essentially half-metallic, while the DOS obtained by HSE features a clear gap in both spin channels—the majority-spin gap being smaller—suggesting that the doped monolayer is a magnetic semiconductor.

We consider next the interaction of two Mn dopant atoms in monolayer MoS_2 (4×4 supercell; 12.5% doping). For brevity, we only discuss the case of Mn dopants in first-nearest-neighbor substitutional sites; the picture is qualitatively the same for second- and third-nearest-neighbor cases. Figures 1(c) and 1(d) display the spin densities at the PBE and HSE levels. By projecting the spin density onto PAW spheres, we obtain average local moments of 1.32 μ_B and 2.86 μ_B on the Mn atoms at the PBE and HSE levels, respectively, indicating that the Mn dopants once again adopt low-spin d^3 and high-spin d^3 configurations depending upon the level of theory employed. The corresponding density of states are displayed in Figs. 2(c) and 2(d); atom-projected DOS are displayed in the Supplementary Material.[33] Upon comparing the PBE results for 6.25% and 12.5% Mn doping, we observe that the doped monolayer is unambiguously half-metallic in the latter case. The three peaks straddling

the Fermi level in the 6.25% Mn case merge into a single broad peak in the 12.5% Mn case. This places the Fermi level within the partially occupied majority band of the impurities occupying only the bonding states while leaving the antibonding minority states unoccupied, which is suggestive of an operative double-exchange mechanism.[4] In the HSE calculations, both spin channels remain semiconducting and the Fermi level remains within the band gap. The impurity d states are still contained within the gap of the host material, which would again suggest that double exchange ought to dominate the exchange coupling. However, the inclusion of a fraction of exact exchange in the HSE functional lowers the energy of the occupied d levels, analogous to previous reports[4] on Mn-doped III-Vs that employ some form of self-interaction correction (e.g., the DFT + U approach,[34–36] SIC-LSD,[37,38] etc.). This would imply a decrease in the strength of the computed exchange coupling constants at the HSE level relative to the PBE situation. As we will show later, this is also manifested in lower Curie temperatures when using HSE-parameterized exchange coupling coefficients relative to the PBE ones.

To estimate the strength of exchange coupling, we report in Table I the energy differences between the ferromagnetic ground state and the metastable antiferromagnetic state (Δ_{AFM-FM}) for two Mn atoms placed at first, second, and third nearest-neighbor Mo sites. These are the only unique neighbor arrangements in a 4 × 4 supercell. At the PBE level, we also report energy differences for first-nearest-neighbor Mn dopants in larger supercells; HSE calculations were not performed for these additional cases due to the enormous computational cost. From the presented data, it is clear that the Mn dopant atoms preferentially display ferromagnetic coupling at both the PBE and HSE level. It is also clear that the HSE functional predicts stronger but shorter-ranged exchange interactions relative to PBE, which is to be expected based on the electronic DOS presented previously. For the various nearest-neighbor configurations studied here, we also report in Table I the relative energy differences between the ferromagnetic ground states (ΔE_{FM}). From these data, we see that the first-nearest-neighbor configuration of Mn dopants is energetically lower by 0.3–0.7 eV (depending upon the level of theory) than the second- or third-nearest-neighbor cases, which suggests a strong thermodynamic driving force for clustering of dopant atoms. While this result would suggest the need for kinetically trapping Mn dopant atoms to produce a uniform, dilute distribution of magnetic impurities, the ability to produce ferromagnetic Mn clusters in the host MoS_2 lattice might also be technologically useful.

TABLE I. Energy differences (Δ_{AFM-FM}) between the ferromagnetic ground state and the antiferromagnetic high-energy metastable state for two Mn dopants placed at identical substitutional sites in the MoS_2 monolayer. Also displayed are energies of the ferromagnetic ground state for different spatial arrangements of Mn atoms (m^{th}-nearest-neighbor) relative to the first-nearest-neighbor configuration ($\Delta E_{FM} = E_{FM}^{m^{th}-nn} - E_{FM}^{1^{st}-nn}$).

		Δ_{AFM-FM} (eV)		ΔE_{FM} (eV)	
Supercell	Configuration	PBE	HSE	PBE	HSE
4 × 4	1^{st} n.n.	0.18	0.22	0.0	0.0
	2^{nd} n.n.	0.06	0.07	0.37	0.66
	3^{rd} n.n	0.03	−0.00	0.43	0.65
6 × 6	1^{st} n.n.	0.17			
8 × 8	1^{st} n.n.	0.17			

B. Monte Carlo simulations

It is well known that ordering in DMSs is strongly influenced by percolation; the mean-field approximation cannot capture this behavior and tends to systematically overestimate the Curie temperature in these systems.[4,36,39–41] Therefore, to allow for a proper description of spatial disorder and magnetic percolation in the Mn/MoS_2 DMS, we parameterized the first-principles exchange interactions between Mn atoms and incorporated these within a Monte Carlo model. The exchange coupling coefficient $J(r)$ is parameterized using the functional form

$$J(r) = \begin{cases} \frac{c}{r^3}\exp[-r/r_0], & \text{if} \quad r \leqslant r_c \\ 0, & \text{otherwise} \end{cases}, \qquad (1)$$

where r is the distance between two impurities, r_0 is the screening length, r_c is the cutoff in the interaction range, and c is a constant of proportionality.[42] The cutoff length was set to the radius of the tenth nearest-neighbor shell (14.48 Å). The remaining parameters were obtained by fitting the energy differences Δ_{AFM-FM} to the model in Eq. (1). The parameters obtained from the fits to the PBE data are $c = 5.965$ eV/Å^3 and $r_0 = 25.957$ Å. The HSE data, while more limited than the PBE set, yield best fit parameters of $c = 12.971$ eV/Å^3 and $r_0 = 4.944$ Å. The exchange coupling energies that result from these parametrizations are displayed in Fig. 3(a), the discrete points representing each neighbor shell up through the cutoff distance. As expected from the data in Table I, the HSE coupling is stronger at first-nearest-neighbor separation but drops off more rapidly than its PBE counterpart. It is worth noting that there are certainly more sophisticated techniques to extract exchange coupling coefficients based on linear response,[43] frozen magnons,[44] etc. Such approaches are beyond the scope of the present work and will be considered elsewhere. For now, the total-energy approach adopted here is sufficient to bring out the principal features of magnetic interactions in DMSs and has adequate precedent in the literature.[35,41]

With the exchange coupling coefficients in hand, it is straightforward to set up a Metropolis Monte Carlo (MC) calculation[45] to simulate the role of disorder and percolation in Mn/MoS_2 DMSs. Briefly, the entire problem was mapped to a Heisenberg model on a triangular lattice, i.e., the underlying lattice formed by the Mo sites.[46] We examined system sizes ranging from 20 × 20 to 100 × 100 containing dopant concentrations ranging from 5% to 15%. Configurational disorder was simulated using 40 different random initial conditions, and all thermodynamic properties were calculated by averaging over these distinct runs. Two procedures were used to estimate the Curie temperature (T_C). In the absence of an external magnetic field, the magnetic susceptibility ($\chi = [\langle M^2\rangle - \langle|M|\rangle^2]/k_BT$) diverges at the critical temperature in the thermodynamic limit. On a finite lattice the susceptibility displays a broadened peak; we use the position of this peak from the largest simulated

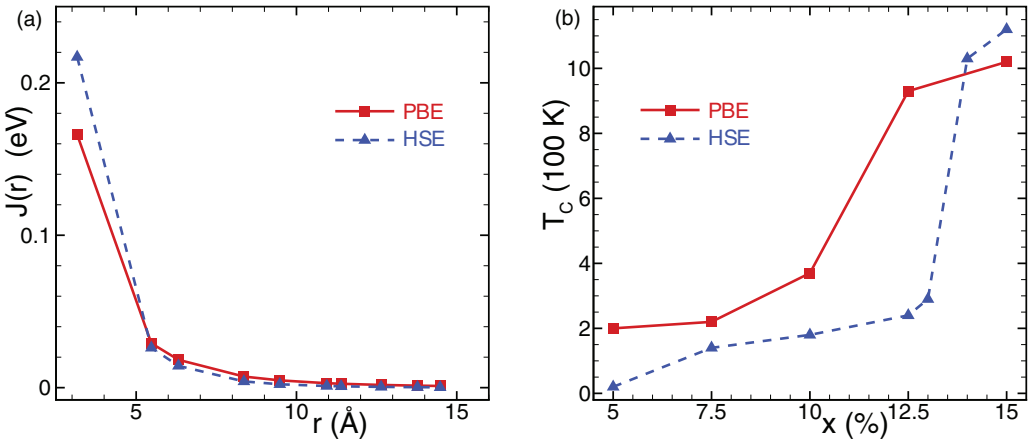

FIG. 3. (Color online) (a) Exchange coupling coefficient obtained from the model in Eq. (1). Symbols correspond to each neighbor shell up to the tenth-nearest neighbor. The HSE exchange coupling is stronger at first-nearest-neighbor separation but drops off more rapidly than its PBE counterpart with increasing distance, which leads to lower Curie temperatures (T_C) in the range of 5–12.5% doping as seen in (b). At sufficiently high concentrations, the stronger nearest-neighbor interaction at the HSE level begins to dominate and leads to higher values of T_C than the PBE-based estimates.

lattice as one estimate of the Curie temperature. The second estimate is obtained from the Binder cumulant method.[47] Binder's cumulant, defined as

$$U_4 = 1 - \frac{\langle m^4 \rangle}{3\langle m^2 \rangle^2}, \tag{2}$$

is only weakly dependent on system size and the common point of intersection of the U_4 versus temperature curves for various system sizes furnishes an estimate of T_C. For our DMSs, we find that the two estimates for T_C are in poor agreement at low dopant concentration, most likely due to lack of percolation in the lattice. At higher concentrations ($\gtrsim$10% for PBE; $\gtrsim$13% for HSE), the two estimates come into better agreement. Here, we choose to consistently use the susceptibility data for estimating T_C. In Fig. 3(b), we display estimates for T_C as a function of dopant concentration using both the PBE and HSE parameterized exchange coupling. As seen from Fig. 3(b), the HSE predictions of T_C are consistently—and often significantly—lower than their PBE counterparts. This is essentially a manifestation of the shorter range of HSE exchange interactions as alluded to before. At a fundamental level, these significant differences underscore the need for functionals that can describe exchange and correlation effects more accurately. We see a sharp increase in T_C beyond 10% and 13% Mn doping at the PBE and HSE levels, respectively, which is most likely indicative of the onset of percolation. The eventual increase in the HSE estimate for T_C as compared to the PBE estimate at 15% doping is due to the stronger nearest-neighbor exchange coupling at the HSE level. Collectively, these results point towards the distinct possibility of achieving room-temperature ferromagnetism in MoS_2 monolayers for Mn doping in the range of 10–15%.

III. CONCLUSIONS

In summary, we conducted a combined DFT and Monte Carlo study of ferromagnetic ordering in Mn-doped monolayer MoS_2. Our DFT studies show that the electronic structure of the resulting DMSs, as well as the strength and range of exchange interactions, are quite sensitive to the level of theory employed. This is most clearly manifested in the lower Curie temperatures obtained with the hybrid HSE XC functional, which corrects for some of the self-interaction error in semilocal functionals through the mixing of a fraction of exact exchange. We find that exchange interactions in Mn/MoS_2 DMSs are primarily governed by the double-exchange mechanism and are relatively short-ranged, making percolation a key factor for magnetic ordering. Based on our DFT-parameterized MC simulations, we predict that dopant concentrations in the range of 10–15% ought to lead to room-temperature ferromagnetism in Mn/MoS_2 DMSs. It remains to be seen whether these predictions can be realized experimentally. At the very least, previous experiments have demonstrated the ability to dope MoS_2 films, nanoparticles, and nanotubes with transition metals such as Re,[48] Ti,[49] Cr,[50] and Mn.[51] Our theoretical predictions will hopefully motivate additional investigations along similar lines with the aim of tailoring the magnetic properties of doped few-layer MoS_2 for novel electronic applications.

APPENDIX: COMPUTATIONAL METHODS

All first-principles calculations were performed using the Vienna *ab initio* simulation package (VASP).[20] The projector-augmented wave (PAW) method[52,53] was used to represent the nuclei plus core electrons. Electron exchange and correlation was treated using both the Perdew-Burke-Ernzerhof (PBE)[21] parametrization of the generalized-gradient approximation as well as the Heyd-Scuseria-Ernzerhof (HSE)[22] hybrid functional. From convergence tests, the kinetic energy cutoff was set at 400 eV; the Brillouin zones for 4×4 supercells were sampled with a $2 \times 2 \times 1$ Γ-centered k-point mesh, whereas a single Γ point was used for larger supercells. A Gaussian smearing of 0.05 eV was employed in conjunction with an energy tolerance of 10^{-4} eV for electronic relaxation. The cell vectors were fixed at the equilibrium value for the MoS_2

monolayer and atomic positions relaxed with a tolerance of 0.01 eV/Å. Periodic images were separated by at least 10 Å of vacuum normal to the monolayer to eliminate spurious interlayer coupling.

*ashwin@engin.umass.edu
†doron.naveh@biu.ac.il

[1] S. A. Wolf, D. D. Awschalom, R. A. Buhrman, J. M. Daughton, S. von Molńar, M. L. Roukes, A. Y. Chtchelkanova, and D. M. Treger, Science **294**, 1488 (2001).
[2] S. J. Pearton, C. R. Abernathy, M. E. Overberg, G. T. Thaler, D. P. Norton, N. Theodoropoulou, A. F. Hebard, Y. D. Park, F. Ren, and J. Kim, J. Appl. Phys. **93**, 1 (2003).
[3] A. H. MacDonald, P. Schiffer, and N. Samarth, Nat. Mater. **4**, 195 (2005).
[4] K. Sato, L. Bergqvist, J. Kudrnovský, P. H. Dederichs, O. Eriksson, I. Turek, B. Sanyal, G. Bouzerar, H. Katayama-Yoshida, and V. A. Dinh, Rev. Mod. Phys. **82**, 1633 (2010).
[5] T. Dietl, Nat. Mater. **9**, 965 (2010).
[6] J. A. Wilson and A. D. Yoffe, Adv. Phys. **18**, 193 (1969).
[7] A. Ramasubramaniam, Phys. Rev. B **86**, 115409 (2012).
[8] Q. H. Wang, K. Kalantar-Zadeh, A. Kis, J. N. Coleman, and M. S. Strano, Nat. Nanotech. **7**, 699 (2012).
[9] A. Ayari, E. Cobas, O. Ogundadegbe, and M. S. Fuhrer, J. Appl. Phys. **101**, 014507 (2007).
[10] B. Radisavljevic, A. Radenovic, J. Brivio, V. Giacometti, and A. Kis, Nat. Nanotech. **6**, 147 (2011).
[11] B. Radisavljevic, M. B. Whitwick, and A. Kis, ACS Nano **5**, 9934 (2011).
[12] Z. Yin, H. Li, H. Li, L. Jiang, Y. Shi, Y. Sun, G. Lu, Q. Zhang, X. Chen, and H. Zhang, ACS Nano **6**, 74 (2012).
[13] J. Zhang, J. M. Soon, K. P. Loh, J. Yin, M. B. Sullivian, and P. Wu, Nano Lett. **7**, 2370 (2007).
[14] S. Mathew, K. Gopinadhan, T. K. Chan, X. J. Yu, D. Zhan, L. Cao, A. Rusydi, M. B. H. Breese, S. Dhar, and Z. X. Shen, Appl. Phys. Lett. **101**, 102103 (2012).
[15] S. Tongay, S. S. Varnoosfaderani, B. R. Appleton, J. Wu, and A. F. Hebard, Appl. Phys. Lett. **101**, 123105 (2012).
[16] Y. Li, Z. Zhou, S. Zhang, and Z. Chen, J. Am. Chem. Soc. **130**, 16739 (2008).
[17] A. R. Botello-Mendéz, F. López-Urías, M. Terrones, and H. Terrones, Nanotechnology **20**, 325703 (2009).
[18] A. Vojvodic, B. Hinnemann, and J. K. Nørskov, Phys. Rev. B **80**, 125416 (2009).
[19] C. Ataca and S. Ciraci, J. Phys. Chem. C **115**, 13303 (2011).
[20] G. Kresse and J. Furthmüller, Comput. Mater. Sci. **6**, 15 (1996); Phys. Rev. B **54**, 11169 (1996).
[21] J. P. Perdew, K. Burke, and M. Ernzerhof, Phys. Rev. Lett. **77**, 3865 (1996).
[22] J. Heyd, G. E. Scuseria, and M. Ernzerhof, J. Chem. Phys. **118**, 8207 (2003); **124**, 219906 (2006).
[23] B. G. Janesko, T. M. Henderson, and G. E. Scuseria, Phys. Chem. Chem. Phys. **11**, 443 (2009).
[24] J. K. Ellis, M. J. Lucero, and G. E. Scuseria, Appl. Phys. Lett. **99**, 261908 (2011).
[25] A closer analysis shows that the Mn dopant has local C_s symmetry, the mirror plane being the plane of the metal atoms.
[26] A. Enyashin, S. Gemming, and G. Seifert, Eur. Phys. J. Spec. Top. **149**, 103 (2007).
[27] T. Boker, R. Severin, A. Muller, C. Janowitz, R. Manzke, D. Voss, P. Kruger, A. Mazur, and J. Pollmann, Phys. Rev. B **64**, 235305 (2001).
[28] T. Li and G. Galli, J. Phys. Chem. C **111**, 16192 (2007).
[29] L. F. Mattheiss, Phys. Rev. B **8**, 3719 (1973).
[30] R. Coehoorn, C. Haas, J. Dijkstra, C. J. F. Flipse, R. A. de Groot, and A. Wold, Phys. Rev. B **35**, 6195 (1987).
[31] P. D. Fleischauer, J. R. Lince, P. Bertrand, and R. Bauer, Langmuir **5**, 1009 (1989).
[32] A. Ramasubramaniam, D. Naveh, and E. Towe, Phys. Rev. B **84**, 205325 (2011).
[33] See Supplemental Material at http://link.aps.org/supplemental/10.1103/PhysRevB.87.195201 for the bandwise, atom-projected decomposition of the total density of states.
[34] S. L. Dudarev, G. A. Botton, S. Y. Savrasov, C. J. Humphreys, and A. P. Sutton, Phys. Rev. B **57**, 1505 (1998).
[35] P. Mahadevan, A. Zunger, and D. D. Sarma, Phys. Rev. Lett. **93**, 177201 (2004).
[36] L. Bergqvist, O. Eriksson, J. Kudrnovský, V. Drchal, A. Bergman, L. Nordström, and I. Turek, Phys. Rev. B **72**, 195210 (2005).
[37] J. P. Perdew and A. Zunger, Phys. Rev. B **23**, 5048 (1981).
[38] T. C. Schulthess, W. M. Temmerman, Z. Szotek, W. H. Butler, and G. M. Stocks, Nat. Mater. **4**, 838 (2005).
[39] L. Bergqvist, O. Eriksson, J. Kudrnovsky, V. Drchal, P. Korzhavyi, and I. Turek, Phys. Rev. Lett. **93**, 137202 (2004).
[40] J. L. Xu, M. van Schilfgaarde, and G. D. Samolyuk, Phys. Rev. Lett. **94**, 097201 (2005).
[41] Y. D. Park, A. T. Hanbicki, S. C. Erwin, C. S. Hellberg, J. M. Sullivan, J. E. Mattson, T. F. Ambrose, A. Wilson, G. Spanos, and B. T. Jonker, Science **295**, 651 (2002).
[42] This model is a modified version of the double-exchange model used in Ref. 4 from which we have dropped the concentration dependence ($\sim 1/\sqrt{c}$) of the prefactor as this requires definitive knowledge of the exchange mechanism. While our results point to a double-exchange mechanism, we do not have sufficient *ab initio* data to firmly establish the concentration dependence of the prefactor. If we were to assume a $1/\sqrt{c}$ dependence when fitting our existing data, this would only serve to increase the exchange coupling at lower concentrations from the present value and raise the Curie temperatures for those low-doping cases. Our overall conclusions, especially in the range of 10% and higher doping, which are of interest for room-temperature ferromagnetism, would essentially remain unaltered.
[43] A. I. Liechtenstein, M. I. Katsnelson, V. P. Antropov, and V. A. Gubanov, J. Magn. Magn. Mater. **67**, 65 (1987).
[44] L. M. Sandratskii and P. Bruno, Phys. Rev. B **66**, 134435 (2002).
[45] N. Metropolis, A. W. Rosenbluth, M. N. Rosenbluth, A. H. Teller, and E. Teller, J. Chem. Phys **21**, 1087 (1953).
[46] More specifically, since any site is either empty ($\sigma = 0$) or accommodates only two distinct spin orientations ($\sigma = \pm 1$) (noncollinear spins are not examined in this study), the Heisenberg model reduces to a three-state Potts model.
[47] K. Binder and D. W. Heermann, *Monte Carlo Simulation in Statistical Physics*, 5th ed. (Springer-Verlag, Heidelberg, 2010).

[48]L. Yadgarov, R. Rosentsveig, G. Leitus, A. Albu-Yaron, A. Moshkovich, V. Perfilyev, R. Vasic, A. I. Frenkel, A. N. Enyashin, G. Seifert, L. Rapoport, and R. Tenne, Angew. Chem. Int. Ed. **51**, 1148 (2011).
[49]W. K. Hsu, Y. Q. Zhu, N. Yao, S. Firth, R. J. H. Clark, H. Kroto, and D. R. M. Walton, Adv. Funct. Mater. **11**, 69 (2001).
[50]T. D. Durbin, J. R. Lince, and J. A. Yarmoff, J. Vac. Sci. Technol. A **10**, 2529 (1992).
[51]J. R. Lince, D. J. Carre, and P. D. Fleischauer, Phys. Rev. B **36**, 1647 (1987).
[52]P. E. Blochl, Phys. Rev. B **50**, 17953 (1994).
[53]G. Kresse and D. Joubert, Phys. Rev. B **59**, 1758 (1999).